*remote sensing*

MDPI

*Article*

# Mapping the Age of Subtropical Secondary Forest Using Dense Landsat Time Series Data: An Ensemble Model

**Shaoyu Zhang [1], Jun Yu [2], Hanzeyu Xu [1,3], Shuhua Qi [1,*], Jin Luo [1], Shiming Huang [2], Kaitao Liao [1,4] and Min Huang [1]**

[1] Key Laboratory of Poyang Lake Wetland and Watershed Research (Ministry of Education), School of Geography and Environment, Jiangxi Normal University, Nanchang 330022, China; zhangsy11600@jxnu.edu.cn (S.Z.); xuhanzeyu@njnu.edu.cn (H.X.); luojin@jxnu.edu.cn (J.L.); huangm@jxnu.edu.cn (M.H.)
[2] Jiangxi Forestry Resources Monitoring Center, Nanchang 330046, China; 13576086527@163.com (J.Y.); isimonhuang@126.com (S.H.)
[3] School of Geography, Nanjing Normal University, Nanjing 210034, China
[4] Key Laboratory of Soil Erosion and Prevention, Jiangxi Academy of Water Science and Engineering, Nanchang 330029, China
* Correspondence: qishuhua11@jxnu.edu.cn

**Abstract:** Quantifying secondary forest age (SFA) is essential to evaluate the carbon processes of forest ecosystems at regional and global scales. However, the successional stages of secondary forests remain poorly understood due to low-frequency thematic maps. This study aimed to estimate SFA with higher frequency and more accuracy by using dense Landsat archives. The performances of four time-series change detection algorithms—moving average change detection (MACD), Continuous Change Detection and Classification (CCDC), LandTrendr (LT), and Vegetation Change Tracker (VCT)—for detecting forest regrowth were first evaluated. An ensemble model was then developed to determine more accurate timings for forest regrowth based on the evaluation results. Finally, after converting the forest regrowth year to the SFA, the spatiotemporal and topographical distributions of the SFA were analyzed. The proposed ensemble model was validated in Jiangxi province, China, which is located in a subtropical region and has experienced drastic forest disturbances, artificial afforestation, and natural regeneration. The results showed that: (1) the developed ensemble model effectively determined forest regrowth time with significantly decreased omission and commission rates compared to the direct use of the four single algorithms; (2) the optimal ensemble model combining the independent algorithms obtained the final SFA for Jiangxi province with the lowest omission and commission rates in the spatial domain (14.06% and 24.71%) and the highest accuracy in the temporal domain ($R^2$ = 0.87 and root mean square error (RMSE) = 3.17 years); (3) the spatiotemporal and topographic distribution from 1 to 34 years in the 2021 SFA map was analyzed. This study demonstrated the feasibility of using change detection algorithms for estimating SFA at regional to national scales and provides a data foundation for forest ecosystem research.

**Keywords:** secondary forest age (SFA); change detection; ensemble model; Landsat time series



**Citation:** Zhang, S.; Yu, J.; Xu, H.; Qi, S.; Luo, J.; Huang, S.; Liao, K.; Huang, M. Mapping the Age of Subtropical Secondary Forest Using Dense Landsat Time Series Data: An Ensemble Model. *Remote Sens.* **2023**, *15*, 2067. https://doi.org/10.3390/rs15082067

Academic Editor: Dino Ienco

Received: 24 March 2023
Revised: 12 April 2023
Accepted: 12 April 2023
Published: 14 April 2023



## 1. Introduction

Forest ecosystems play an important role in the carbon cycle by regulating atmospheric $CO_2$ [1,2] and can be used to achieve carbon neutrality [3]. Understanding forest dynamics, and, particularly, the extent of secondary forests, is key to the integrity of forest landscapes and carbon accumulation [4,5]. A secondary forest is an important forest or woodland ecosystem that develops without evident disturbance through regeneration or afforestation. Compared to other forest types, secondary forests have higher productivity and carbon sequestration rates [6]. Thus, there is a need to quantitatively understand the structure of secondary forests [7].

The stand age of regeneration or afforestation areas is an important indicator of the patterns, regrowth range, and extent of secondary forests. In general, stand age is a critical factor in determining the carbon stocks of a forest ecosystem and their fluxes at various spatiotemporal scales [8–15]. In particular, SFA has a great impact on net primary production [13,16]. Characterization of SFA often relies on a fieldwork-based forest inventory. Recently, remote sensing-based SFA mapping has been proven effective at both the regional and local scales [17–21].

Various thematic datasets have been produced to analyze SFA using remote sensing techniques and other methods. SFA is commonly obtained by detecting the change in multi-temporal land cover maps [22–24]. Classification-based SFA mapping offers an alternative approach that provides sufficient spatial details from high-resolution images [18,25–29]. The relationship between the sampling age and relevant biological information derived from satellite images can also be used to quantitatively estimate parameters of large-scale secondary forests, such as forest structure parameters, aboveground canopy height, biomass, and gross primary productivity [19,30]. However, these methods are not able to provide fine-scale, accurate results due to the limited land cover maps, images, and inventory data available for sub-tropical regions [31,32].

Among the alternative datasets, Landsat archives are optimal for mapping SFA due to their fine resolution and the fact that they have the longest periods of monitoring [33]. Various time-series change detection algorithms have been proposed to make full use of available Landsat images. These algorithms have been proven effective for capturing frequent forest disturbances and include the VCT [34,35], LT [36,37], and CCDC [38,39]. These algorithms can be broadly divided into six categories according to differences in application and preprocessing [40]: (1) thresholding, (2) differencing, (3) segmentation, (4) trajectory classification, (5) statistical boundary, and (6) regression. For example, the thresholding method is controlled by the specification of an accurate threshold; the differencing method can identify irregular events over time using large differences between places; the segmentation method needs all the historical time-series data; trajectory classification is less ideal for the detection of abrupt changes; setting a statistical boundary results in a high commission rate; the regression method is only functional with a clear trend. Recently, a fusion approach has been recommended to overcome the drastic differences in the results obtained by the different algorithms. The fusion approach detects disturbances rather than only one algorithm or index being used [41–43]. However, there remains a need to assess the performances of these individual algorithms and ensemble approaches in the detection of forest regrowth, although these algorithms have been further used to detect other land disturbances resulting from the planting of cash crops and urbanization [22,44–47].

The present study aimed to effectively apply time-series change detection algorithms to map SFA using dense Landsat archives. The relative performances of four time-series change detection algorithms in detecting forest regrowth were first evaluated. An ensemble model that could obtain more accurate timings for secondary forest regrowth was then developed to map the SFA. The ensemble model was validated for Jiangxi province, China. This province falls in a subtropical climate zone and has experienced frequent forest disturbances, artificial afforestation, and natural regeneration over the past four decades. The spatiotemporal and topographical distributions of the final 2021 SFA map for Jiangxi province from 1 to 34 years were analyzed. Secondary forest was defined as regrowth forest during the period from 1987 to 2020 in this study. The current study can provide an improved understanding of the development of subtropical secondary forests.

## 2. Materials and Methods

### *2.1. Study Area*

The study area for the present study was Jiangxi province (113°35′–118°29′E, 24°29′–30°05′N), China, on the south bank of the middle and lower reaches of the Yangtze River, encompassing an area of $16.69 \times 10^4$ km$^2$. Jiangxi province contains 11 prefecture-level cities;

namely, Ganzhou (GZ), Ji'an (JA), Fuzhou (FZ), Xinyu (XY), Pingxiang (PX), Yichun (YC), Nanchang (NC), Yingtan (YT), Shangrao (SR), Jingdezhen (JDZ), and Jiujiang (JJ) (Figure 1b). The province falls in a subtropical humid monsoon climate zone with a temperature range of 16 to 19 °C, abundant rainfall, and a relatively long frost-free period. Jiangxi province plays the role of ecological protective screen for the provinces located in the north of China due to its superior climatic conditions, abundant biological resources, and complex topographic conditions. It is also a critical area under the protection of "Green Waters and Green Mountains", which is China's current major strategy for environmental governance and protection.

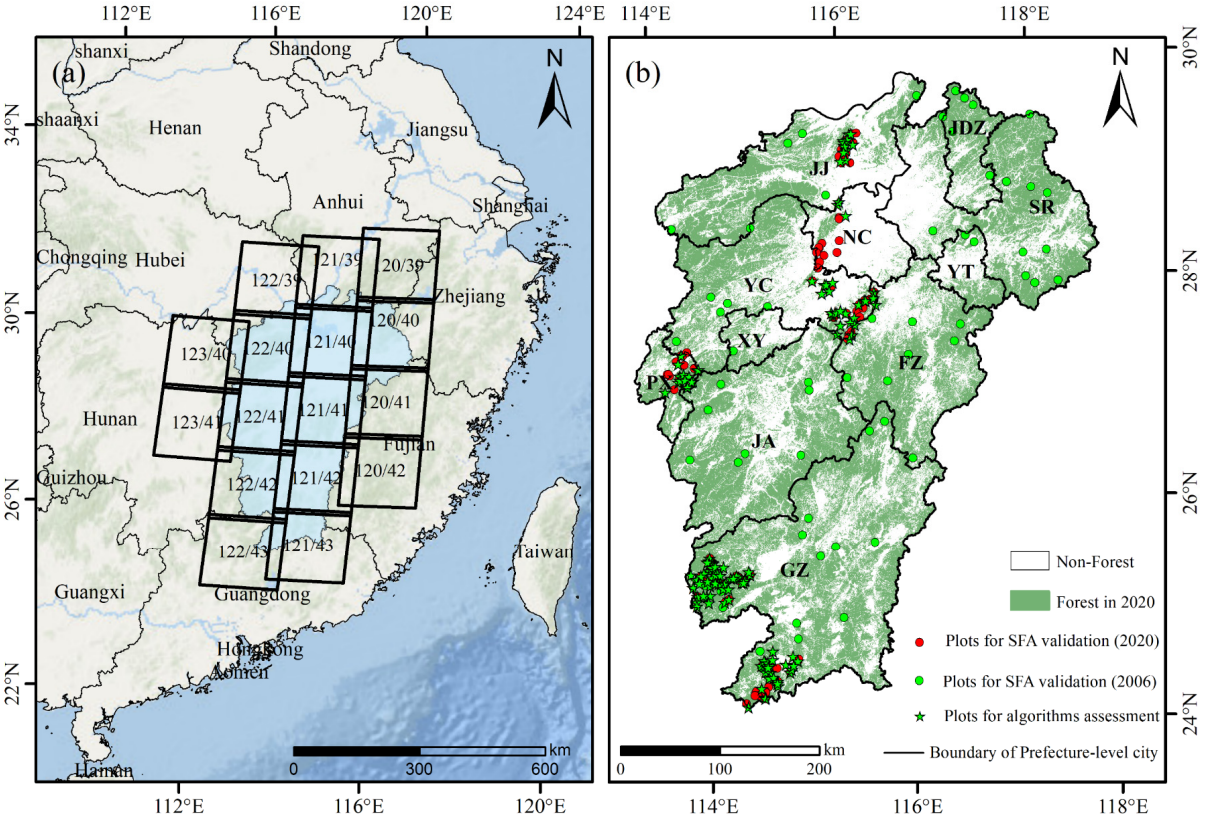


**Figure 1.** Map of the study area. (**a**) The location of Jiangxi province in China and its corresponding Landsat scenes (black rectangles). (**b**) The new reference forest map of Jiangxi province in 2020 (described in Section 2.2.3) and the forest samples (described in Section 2.2.2).

Forests in Jiangxi province have experienced extensive disturbances, with initial large-scale deforestation changing to forest conservation in recent years. Many forests were destroyed from 1956 to 1966 to provide fuel for the steel smelting industry. By the 1970s, the total area of forest in Jiangxi province had decreased to 31.5% of the total land area. However, many dominant species, such as *Cunninghamia lanceolate*, *Pinus elliottii*, and *Pinus massoniana*, were subsequently planted, extending the forest coverage in Jiangxi province to 61.16% in 2018, the second highest in China (China Forest Resources Report, 2014–2018) [48]. Large-scale artificial afforestation and natural regrowth have increased the importance of secondary forests in Jiangxi province. Under the strict supervision and management system for liability drafted by the Jiangxi government, planted trees will be nurtured and sealed in the coming years and not felled in a tree rotation period. The deforested areas are mainly the economic forests planted in early times that arrived at tree rotation or cutting age. The good growth circumstances for secondary forests provided a foundation for detecting the timing of forest regrowth in our study area.

### *2.2. Data and Processing*

#### 2.2.1. Landsat Time-Series Images

The present study used Landsat Collection 1 Level 1 data to detect forest regrowth. These data included the atmospherically corrected surface reflectance data from Landsat 5 Thematic Mapper (TM), Landsat 7 Enhanced Thematic Mapper (ETM+), and Landsat 8 Operational Land Imager (OLI), accessed from the United States Geological Survey (USGS) via Google Earth Engine (GEE) [49]. The cloud pixels were masked using CFMask [50]. All images from the GEE collections LANDSAT/LC08/C01/T1_SR, LANDSAT/LE07/C01/T1_SR, and LANDSAT/LT05/C01/T1_SR were selected based on the study area (Figure 1a) and study period (from 1986 to 2021).

#### 2.2.2. Forest Samples for Assessment of Algorithms and Ensemble Models and Validation of SFA Map

The first group's forest samples were used in the assessment of the four individual algorithms and five ensemble models and the second for validation of the SFA map (Table 1 and Figure 1b). These samples were obtained from the Seventh Jiangxi Province Forest Resources Second Class Survey (FRSS) in 2020 and the Sixth National Forest Resources Inventory (NFRI) in 2006 (http://ly.jiangxi.gov.cn/ (accessed on 1 May 2022)). The FRSS and NFRI currently provide the most detailed and highest-quality data available in China for use as field validation data for forest remote sensing [51,52]. The forest age was determined using a visual inspection method based on bark color, height, shape, species, and afforestation time in the field surveys. The FRSS has been conducted every ten years since the 1950s, and the Seventh FRSS, updated on 31 December 2020, recorded information on tree species, forest age, tree stock, etc., in each forest patch based on the natural state at the provincial scale. The NFRI also provides forest information for each square plot (25.82 m × 25.82 m), which are systematically allocated based on a grid of 2 km × 4 km at the national scale [53]. The reference data were selected and transformed according to the selection criteria given in Table 1. Only partial reference data covering Jiangxi province were obtained because of data confidentiality (Figure 1b).

**Table 1.** Reference data used for assessment of the algorithms and ensemble models and validation of the SFA map.

| Reference Data Name | Type | Number | Selection Criteria | Properties | Purpose | Source/Provider |
|---|---|---|---|---|---|---|
| First group | Forest patch (Linban in 2020) | 132 | Area $\geq$ 4500 m$^2$<br>Length $\geq$ 60 m<br>Width $\geq$ 60 m | 85 secondary forest points (age $\leq$ 34)<br>47 stable forest points (age $\geq$ 40) | Assessment of four individual algorithms and five ensemble models | Seventh Jiangxi Province Forest Resources Second Class Survey (FRSS) (http://ly.jiangxi.gov.cn/ (accessed on 1 May 2022)) |
| Second group | Forest patch (Linban in 2020) | 65 | Area $\geq$ 4500 m$^2$<br>Length $\geq$ 60 m<br>Width $\geq$ 60 m | Age $\leq$ 34 | Validation of SFA map | Seventh FRSS |
| | Forest plots in 2006 | 95 | 25.82 m × 25.82 m (random sample) | Age $\leq$ 19 | | Sixth National Forest Resources Inventory (NFRI) (http://ly.jiangxi.gov.cn/ (accessed on 1 May 2022)) |

The first group of 132 forest samples from the Seventh FRSS in 2020 was used to assess the performances of the algorithms and ensemble models in detecting forest regrowth. These samples consisted of 85 secondary forest points and 47 stable forest points from the FRSS. The second group of only 160 secondary forest samples was used to evaluate the accuracy of the SFA map and included 65 samples from the Seventh FRSS and 95 samples from the Sixth NFRI. These secondary forest samples were double-checked by sight using historical Landsat and GF-1 and GF-6 panchromatic/multispectral (PMS) images from the China High Score Special Project. Landsat Explorer was also used to examine the change

time for each sample (https://jstnbraaten.users.earthengine.app/view/landsat-timeseries-explorer (accessed on 1 June 2022)). Stable forest samples for the years 2000, 2010, and 2020 were examined with GlobeLand30 [54].

#### 2.2.3. Land Cover Datasets

Three land cover datasets were used to produce a basic forest map for 2020 at 30 m resolution, including World Cover 2020 (ESA-2020), ESRI 2020 Land Cover (ESRI-2020), and GlobeLand30 for 2020 (GLC-2020). The ESA-2020 dataset contains 11 land cover categories and has 10 m resolution, with an overall accuracy (OA) for Asia of 80.7% and a product accuracy (PA) for forests of 92.3% (https://viewer.esa-worldcover.org/worldcover/ (accessed on 1 May 2022)) [55]. ESRI-2020 is a 10 m global land cover map containing ten land cover categories (https://livingatlas.arcgis.com/landcover/ (accessed on 1 May 2022)) [56]. GLC-2020 is a 30 m global land cover product for 2020 with an overall accuracy of 85.72% (http://www.globallandcover.com/ (accessed on 1 May 2022)) [54].

The basic forest map of Jiangxi province in 2020 was obtained by superimposing the ESA-2020, ESRI-2020, and GLC-2020 land cover datasets. The attribute of a pixel was determined depending on whether it was classified as forest by at least two land cover products. The present study visually interpreted 500 forest points obtained from high-resolution images derived from GF-1 and GF-6 PMS images. These interpreted points were used to assess the accuracy of the forest maps. The accuracies of forest areas in the ESA-2020, ESRI-2020, and GLC-2020 datasets and the basic forest map were 88.57%, 84.29%, 85.71%, and 94.29%, respectively (Figure 1b).

#### 2.2.4. Statistical Data for the Area of Artificial Afforestation

Statistical areas of artificial afforestation in Jiangxi province from 1986 to 2020 were compared to the area of secondary forest estimated from 1987 to 2020 in the present study. Statistical data starting from 1986 (one year ahead) were used to address the difficulty of detecting signals of short recovery. Afforestation can be detected from space after a minimum of one year following the afforestation activity when the regeneration is manmade. The data were manually collected and organized from the Forestry Statistical Yearbook published by the Jiangxi Provincial Bureau of Statistics (http://tjj.jiangxi.gov.cn/col/col38595/index.html (accessed on 15 June 2022)) and the Jiangxi Provincial Department of Forestry (http://agri.ckcest.cn/specialtyresources/scientificinfo/detail/1/727636d8-d534-11e9-af7d-0242ac110002.html (accessed on 15 June 2022) and http://agri.ckcest.cn/specialtyresources/scientificinfo/detail/1/7279c2bc-d534-11e9-af7d-0242ac110002.html (accessed on 15 June 2022)).

#### 2.2.5. Auxiliary Data

The auxiliary data used in the present study included elevation data obtained from the NASA Shuttle Radar Topography Mission (SRTM) Version 3.0 [57] and maps of global planting years of plantations (GPYP) [58]. The GPYP dataset is organized in GeoTiff format with 30 meter spatial resolution and can be downloaded at https://figshare.com/articles/dataset/A_global_map_of_planting_years_of_plantations/19070084 (accessed on 1 July 2022). The topographical characteristics of the SFA were analyzed using SRTM data. More details on the datasets used in this study can be found in Table A1.

### *2.3. Methods*

Mapping of SFA in the current study was implemented in four steps: (1) forest regrowth was detected using time-series change detection algorithms; (2) an ensemble model for more accurate estimation of SFA was developed; (3) the quality of the SFA acquired by the four individual algorithms and ensemble models was assessed; (4) analysis based on the final SFA map was conducted. First, forest regrowth time was detected using the four individual time-series change detection algorithms from 1987 to 2020. Each result was assessed using assessment samples (Section 2.2.2). Five ensemble models were then

constructed using the stacked generation approach described below. The optimal ensemble model was used to generate the final 2021 SFA. Lastly, the final SFA map was validated using validation and statistical data (Figure 2).

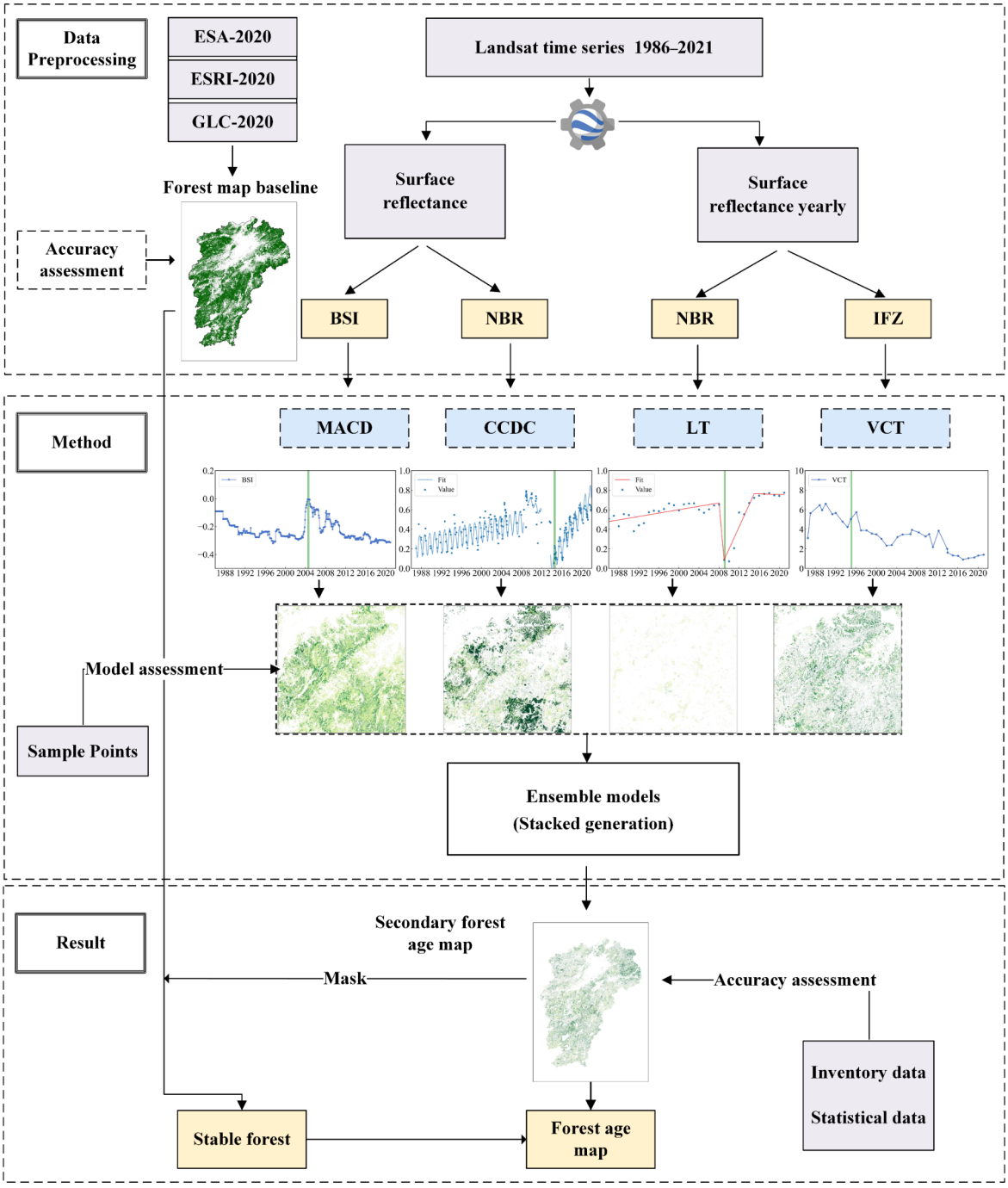


**Figure 2.** A flowchart illustrating the methodology used in the present study for mapping secondary forest age (SFA) in Jiangxi province. Abbreviations: World Cover 2020 (ESA-2020), ESRI 2020 Land Cover (ESRI-2020), GlobeLand 30 for 2020 (GLC-2020), bare soil index (BSI), normalized burn ratio (NBR), integrated forest Z-score (IFZ), moving average change detection (MACD), Continuous Change Detection and Classification (CCDC), LandTrendr (LT), Vegetation Change Tracker (VCT).

#### 2.3.1. Detecting Forest Regrowth Time Using Time-Series Change Detection Algorithms

Four time-series change detection algorithms were used to detect forest regrowth time, including moving average change detection (MACD), Continuous Change Detection and

Classification (CCDC), LandTrendr (LT), and Vegetation Change Tracker (VCT). The latest changes were assumed to be forest regrowth. These algorithms were chosen in the present study due to their wide use in previous studies relating to SFA [22,44,45,59].

1. Moving average change detection (MACD) is a thresholding method in which changes are defined as large deviations from the set threshold. In the present study, MACD considered the moving averages of multiple observations (often three times or more), using all Landsat data (high frequency) to remove abnormal observations by averaging adjacent observations. MACD uses the bare soil index (BSI) [45]. The threshold for detecting forest regrowth was set as −0.026, determined from the 95% confidence interval according to the secondary forest samples;
2. Continuous Change Detection and Classification (CCDC) [38] was used to detect the final change. The normalized burn ratio (NBR) [60] was used as the detection index, aided by the GEE-CCDC-Tools repository (https://gee-ccdc-tools.readthedocs.io/en/latest/# (accessed on 1 July 2022)) [61];
3. LandTrendr (LT) was used to define the forest recovery time based on the property of the recovery trend in LT. This method identifies gradual changes (mainly recovery) in time series by using temporal segmentation and linear regression [36,37]. Yearly surface reflection (SR) composites for input into the LT and VCT algorithms were obtained using the best available pixel (BAP) method, thereby overcoming the influences of cloud and data noise [62]. The NBR was used as the main change index due to its direct response to forest change [63,64];
4. Vegetation Change Tracker (VCT) [34,35] was used to detect forest regrowth based on the integrated forest Z-score (IFZ) threshold. Forests were defined as areas in which the IFZ for a pixel was less than 4.8 for two consecutive years. VCT is an offline and univariate approach requiring considerable computing resources. Therefore, the online VCT was implemented in the present study due to the need for more convenience at the regional level. The IFZ was calculated using the annual cloud-free composite SR (medium frequency) and input into the VCT algorithm to track forest changes at each pixel [65]. The 95% confidence interval was used to determine a VCT threshold of 4.8.

All four algorithms mentioned above were used to detect forest regrowth. Table 2 provides a detailed list of the parameters for each algorithm.

**Table 2.** Parameters of the four algorithms used in this study.

| Algorithm Name | Temporal Frequency | Change Index | Parameter | Category | References |
|---|---|---|---|---|---|
| Moving average change detection (MACD) | All available Landsat data (high frequency) | BSI | Windows = 12<br>Threshold = −0.026 | Threshold | [45] |
| Continuous Change Detection and Classification (CCDC) | All available Landsat data (high frequency) | NBR | minObservations = 6<br>chiSquareProbability = 0.99<br>minNumOfYearsScaler = 1.33<br>dateFormat = 1<br>lambda = 0.002<br>maxIterations = 10,000 | Statistical boundary | [38] |
| Vegetation Change Tracker (VCT) | Medium frequency (06.01–10.20) | IFZ | Threshold = 4.8 | Threshold | [34] |
| LandTrendr (LT) | Medium frequency (06.01–10.20) | NBR | maxSegments = 6<br>spikeThreshold = 0.9<br>vertexCountOvershoot = 3<br>recoveryThreshold = 0.25<br>pvalThreshold = 0.05<br>bestModelProportion = 0.75<br>minObservations = 6 | Regression | [36,37] |

#### 2.3.2. Proposing an Ensemble Model for More Accurate Estimation of SFA

The present study developed ensemble models based on a stacked approach according to the lower omission and commission rates of the individual algorithms. The results of

each algorithm were obtained in GEE and the ensemble models were constructed with different orders of results from the individual algorithms. For example, in the ensemble scheme, VCT + CCDC represents the overwriting of the results from VCT with CCDC. The results from VCT were then retained at the pixels where the changes in the secondary forest were not detected by the CCDC. Five ensemble schemes—VCT + CCDC, CCDC + VCT, CCDC + VCT + LT, CCDC + VCT + MACD, and VCT + CCDC + MACD—were constructed, considering the algorithm assessment results, to estimate SFA. The last period of forest regrowth detected by each algorithm was transformed into the pixel-scale SFA for 2021. For example, the age of 2 in the 2021 SFA map indicates the distribution of forest regrowth detected in 2019.

#### 2.3.3. Accuracy Assessment of SFA Acquired from Algorithms and Ensemble Models

The SFAs computed by all algorithms and ensemble models were assessed based on the 132 forest samples (Section 2.2.2). The performances of the algorithms and ensemble models were evaluated based on the commission rate and omission rate:

$$CR = FP/(TP + FP) * 100 \quad (1)$$

$$OR = FN/(TN + FN) * 100 \quad (2)$$

where *CR* is the commission rate and *OR* is the omission rate, and *CR* and *OR* are the percentage expressions of the commission error and omission error, respectively; *FP* is the number of detected samples in the reference data with false changes; *TP* is the number of samples detected in the reference data with true changes; and *FN* and *TN* are the numbers of reference samples missed and detected in the map, respectively. The true pixels were defined as pixels in which deviation did not exceed ±2 years.

#### 2.3.4. Evaluation of the SFA Map

The SFA map of Jiangxi province was evaluated using 160 secondary forest validation samples and statistical data on artificial afforestation (Sections 2.2.2 and 2.2.4). All forests older than 34 were considered primeval or stable forests, whereas the younger forests were classified as secondary forests in this study. The estimated SFA was compared with the secondary forest sample age using the root mean square error (RMSE) and $R^2$ with linear regression. The area of forest regrowth for each year since 1987 was compared with the statistical area of artificial afforestation (Section 2.2.4).

## 3. Results

### *3.1. Accuracy Assessment of SFA Acquired by the Four Individual Algorithms and Ensemble Models*

According to the 132 forest samples in the first group of reference data listed in Table 1, among the individual algorithms, CCDC achieved the best performance, with omission and commission rates of 37.65% and 15.69%, respectively (Figure 3) (Table A2). LT provided unsatisfying results, with the largest omission rate of 93.75% and a commission rate of 16.28%. MACD obtained the lowest omission rate but a higher commission rate (7.29% and 38.2%, respectively). VCT presented a lower commission rate of 16.28% and a higher omission rate of 49.41%, underperforming slightly compared to CCDC. The ensemble models showed better performances than the independent algorithms in detecting forest regrowth. The ensemble model of CCDC + VCT effectively reduced the omission and commission rates to 14.06% and 24.71%, respectively. Since MACD had a low omission rate, CCDC + VCT + MACD could more successfully minimize the omission rate compared to VCT + CCDC. Results from the ensembles were affected by the stacked order of algorithms. For example, the performance of CCDC + VCT was superior to that of VCT + CCDC, showing a lower commission rate. The optimal performance was obtained by the ensemble model CCDC + VCT + LT, which had the lowest commission and omission rates among all

the ensemble models of 13.85% and 23.53%, respectively (Table A2). As a result, the present study considered the ensemble model CCDC + VCT + LT to be optimal for the estimation of SFA among the five models.

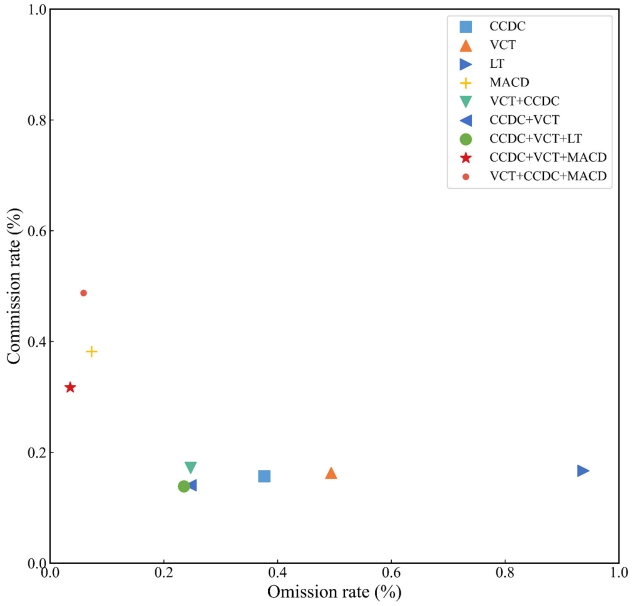


**Figure 3.** Performances of the algorithms and ensemble models. The commission rate and omission rate are lower at points closer to (0,0).

The results showed that all the individual algorithms seldom achieved optimal detection results (Figure 4). For example, while CCDC, LT, and MACD successfully detected the breakpoints in 2004, while VCT did not (Figure 4a5), VCT outperformed the other three algorithms in detecting forest regrowth (Figure 4b5). In addition, the forest regrowth identified by VCT had a two-year lag relative to MACD and CCDC (Figure 4c5). With incomplete removal of the aboveground biomass, CCDC showed an improved ability to detect the breakpoints compared to the other three algorithms (Figure 4d5). MACD only occasionally provided accurate results (Figure 4b5,d5). The timing of forest regrowth was visually presented in the four plots using RGB images from historical Landsat images composed of the red, green, and blue bands. Persistent or stable forests were identified by no forest changes occurring during the study period.

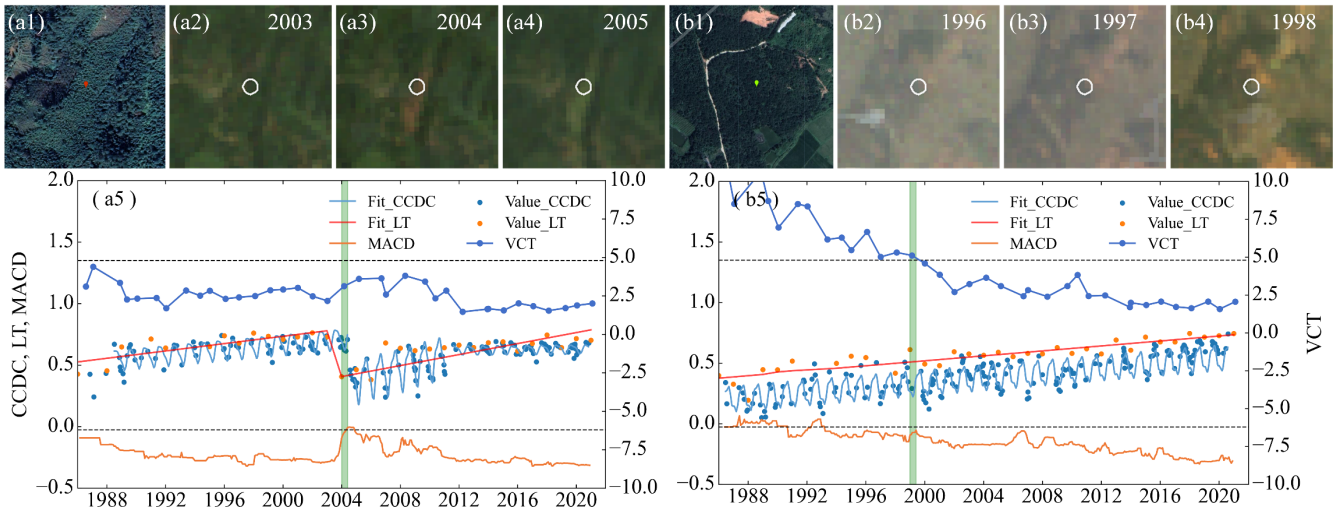


**Figure 4.** *Cont.*

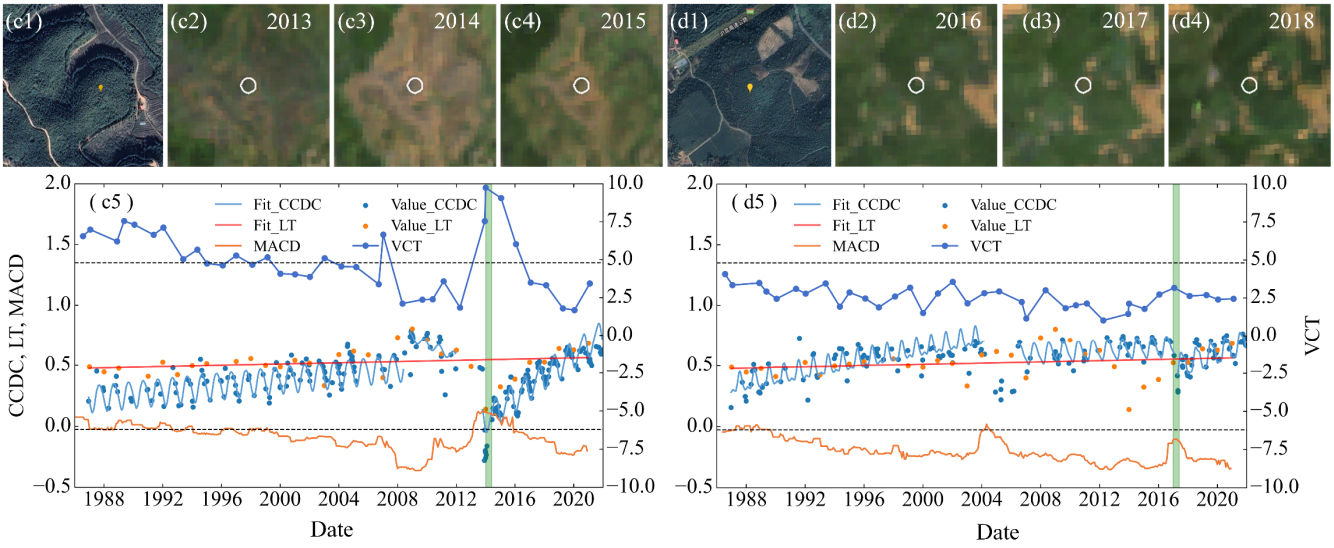


**Figure 4.** Detection of forest regrowth using the moving average change detection (MACD), Continuous Change Detection and Classification (CCDC), LandTrendr (LT), and Vegetation Change Tracker (VCT) algorithms for four forest sampling plots (**a1**) 25°50′39.12″N, 114°8′39.48″E; (**b1**) 27°53′26.16″N, 116°28′45.84″E; (**c1**) 24°47′57.48″N, 114°52′59.52″E; (**d1**) 27°45′47.09″N, 114°9′19.08″E. (**a5**,**b5**,**c5**,**d5**):The left y-axis represents CCDC, LT, and MACD, whereas the right y-axis represents VCT. The thresholds of VCT and MACD are the upper and lower black dashed lines, respectively. (**a2–a4**, **b2–b4**, **c2–c4**, **d2–d4**): The red–blue–green (RGB) images were composed of the red, green, and blue bands from Landsat images.

### *3.2. Validation of the SFA Map*

The forest age determined from the 160 forest samples in the second group listed in Table 1 was used to validate the SFA map. A significant correlation between the estimated and the recorded forest age was identified. The fitted linear regression line was very close to the 1:1 line, with $R^2$ = 0.87 and RMSE = 3.17 (years) (Figure 5).

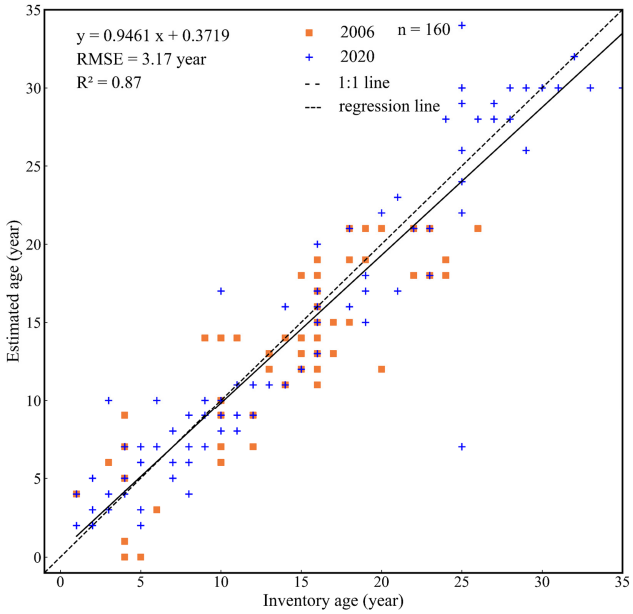


**Figure 5.** Comparison of inventory SFA and estimated SFA.

A comparison between the artificial afforestation area in the statistical data and the estimated forest regrowth area showed that the annual change in statistical afforestation

area was consistent with the area of estimated forest regrowth from 1987 to 2020 (Figure 6). A one-year lag gap between the artificial afforestation and estimated forest regrowth time can be seen in Figure 6. The comparison showed correlations, with $R^2$ = 0.46 for 1987–2020 and $R^2$ = 0.7 for 2000–2020 and a delay of a year for the statistical data. This showed that the SFA map from the ensemble model with CCDC + VCT + LT was reasonable and reliable. The annual average area of estimated forest regrowth was 1627.80 $km^2$, close to the statistical annual average for the artificial afforestation area from 1986 to 2019 in Jiangxi province of 1668.89 $km^2$. The statistical afforestation data and the detected forest regrowth area were successful in showing the continual decreasing trend in the afforestation area since 2009.

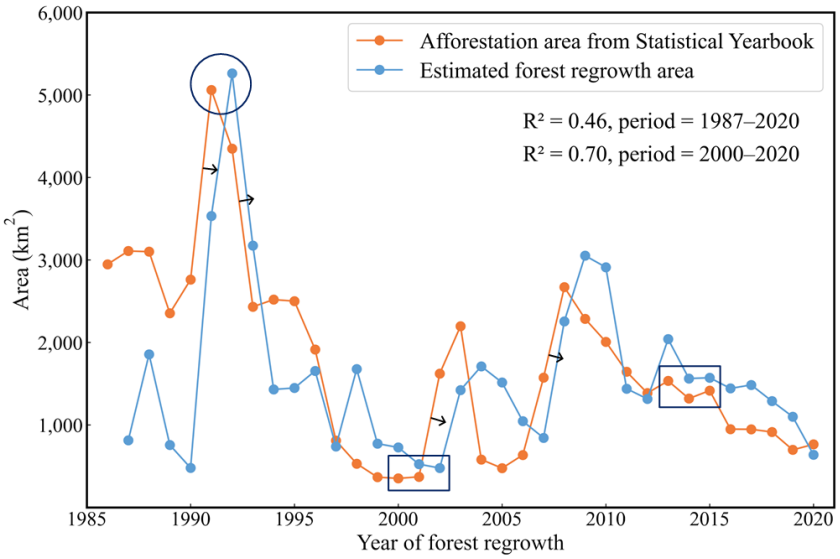


**Figure 6.** Comparison of the statistical afforestation area and estimated forest regrowth area.

Moreover, the area of forest regrowth was underestimated for 1987–1990 and 1994–1997, respectively. Many commercial trees and tree crops have been planted in Jiangxi province with shorter harvest rotations due to intensive management [66]. Harvest rotation indicates the planted forest may be chopped down and reforested after reaching its cutting age. For example, the cutting ages of *Cunninghamia lanceolate* and *Pinus massoniana* in southern mountainous and hilly areas are 11–21 and 16–26 years, respectively, according to the Regulations for Age-class and Age-group Division of Main Tree-species in the Forestry Industry Standard of the People's Republic of China (LY/T 2908-2017). This reveals why a significant difference existed between the statistical artificial and estimated forest regrowth areas in the early period. One main cause may have been that the early-planted forest was chopped down and reforested in recent years to meet the needs of socioeconomic development [67].

The spatial information gained from the four investigated forest plots further validated the SFA map. These additional characteristics included a Google Earth image, an unmanned aerial vehicle (UAV) image, and time series from the change detection algorithms. Figure 7 shows the spatial consistency in the field images, satellite images, and estimated results in four typical forest plots. The UAV images were used to show the growth condition in 2020, whereas the time series from VCT, LT, or CCDC show the process of forest regrowth. The forest regrowth in 2017 for the first plot was detected by the LT algorithm in the ensemble model (Figure 7b4). Figure 7c4 shows forest regrowth in 2009 in the second forest plot detected by the LT algorithm. As shown in Figure 7d4, although the LT algorithm failed to detect forest change for the third forest plot, the change was detected by the VCT algorithm. The fourth forest plot was selected to show a stable forest in which no change was detected by the ensemble model. The fit of the CCDC time series illustrated the stability of the forest plot (Figure 7e4). Overall, the capabilities of the different algorithms for the detection of the

stands of varied secondary forests further explain why the CCDC + VCT + LT ensemble model obtained the optimal results in the present study.

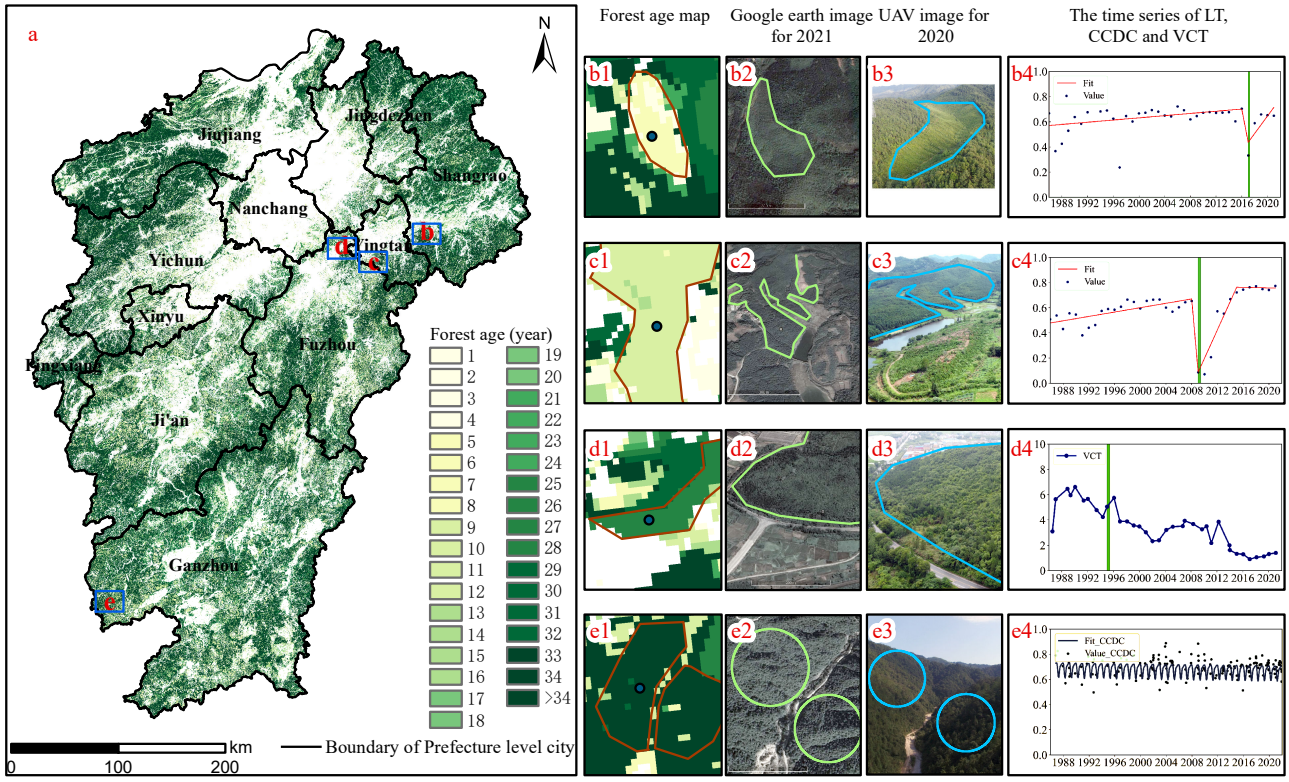


**Figure 7.** (**a**): The spatial distribution of SFA in Jiangxi province in 2021; (**b**–**e**) presents the types of younger, middle-aged, premature forests, and mature forests. The no 1–4 in (**b**–**e**) presents the age results, Google earth images, unmanned aerial vehicle (UAV) images, and time series from the individual algorithms, respectively.

### *3.3. Spatial and Temporal Distributions of SFA*

Figure 7a shows the spatial distribution of SFA in 2021 mapped from the ensemble model with CCDC + VCT + LT. The secondary forest in Jiangxi province over the last 34 years was mainly distributed in the central, southwestern, and southern regions. The secondary forests in northwestern and northeastern Jiangxi province were older than those in southwestern and southeastern Jiangxi province. Prior to 2000, numerous *Pinus massoniana* and *Pinus elliottii* trees were planted in northwestern and northeastern Jiangxi province, with the majority surviving to this day. However, the secondary forests in the southwestern area were mainly represented by artificially planted *Cunninghamia lanceolate* and other cultivated trees; in southeastern Jiangxi province, secondary forests were mainly represented by other cultivated trees, tree crops, and various fruits trees.

Age classes for forest areas in the SFA map were enumerated. The results showed that secondary forests with ages of 28, 29, and 30 years accounted for the largest forest areas and that the maximum areas of forest regrowth were found in 1993, 1992, and 1991 (Figure 8). The average and median ages of the secondary forest were 18 and 17 years, respectively. Secondary forests with small areas aged 19–24 and 31–34 years were identified, and it is highly likely that these forests were deforested in recent years. There was a decreasing trend for the area of forest regrowth, mainly due to the slow artificial afforestation in recent decades due to higher current forest coverage.

The present study divided forests into five age groups. The SFA map indicated the forest area to be $10.09 \times 10^4$ km$^2$, accounting for 60.47% of the total provincial land area. The five age groups comprised mature forests older than 34 years ($4.697 \times 10^4$ km$^2$), mature forests with an age of 31 < age $\leq$ 34 years ($0.391 \times 10^4$ km$^2$), premature forests with an age of

21 < age ≤ 30 years ($2.042 \times 10^4$ km$^2$), middle-aged forests with an age of 11 < age ≤ 20 years ($1.576 \times 10^4$ km$^2$), and forests younger than 10 years ($1.389 \times 10^4$ km$^2$). Figure 9(JX) shows the proportions of the forest areas in different age groups for Jiangxi province, whereas the remaining 11 pie charts in Figure 9 show the areas of forests in different age groups for prefecture-level cities. The total area of secondary forest was estimated to be $5.397 \times 10^4$ km$^2$, accounting for 53.47% and 32.3% of the total forest and total land areas of Jiangxi province, respectively. The area of premature forest was the largest among the secondary forest groups, accounting for 37.8% of the total area.

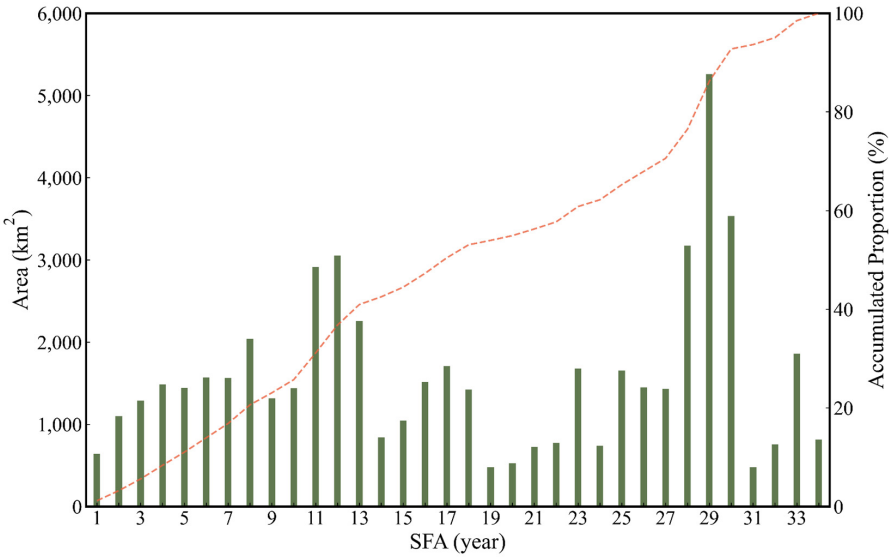


**Figure 8.** Area age classes in the 2021 SFA map in Jiangxi province. The orange dotted line represents the accumulated proportion of SFA.

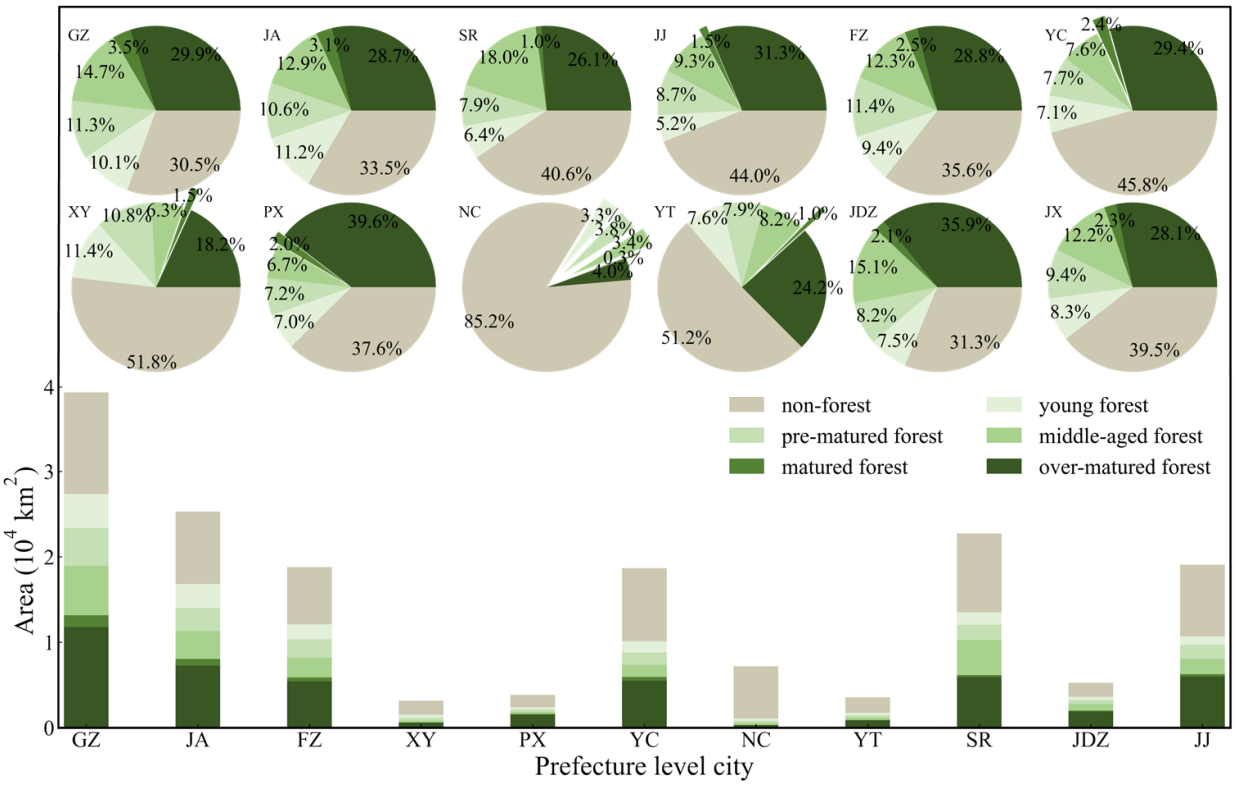


**Figure 9.** Forest area age groups for prefecture-level city divisions.

### *3.4. Topographical Characteristics of SFA*

The characteristics of the SFA differed among the different topographical intervals. The land cover area for each interval decreased significantly with increasing elevation. In addition, over 30% of the land in Jiangxi province has an altitude of less than 100 m above sea level (Figure 10). The proportion of forest area increased with increasing altitude. An analysis of the overlay of elevation and SFA showed that over 80% of forests and 86% of secondary forests in Jiangxi province are at an altitude less than 500 m. The largest forest area was in the elevation interval of 100–200 m, and forest area decreased with increasing altitude. The proportion of secondary forests in the forest area decreased with increasing altitude at altitudes below 800 m. This result could be attributed to increasing and more frequent human activities and more artificial afforestation at lower altitudes. However, the proportion increased with increasing altitude at altitudes exceeding 800 m.

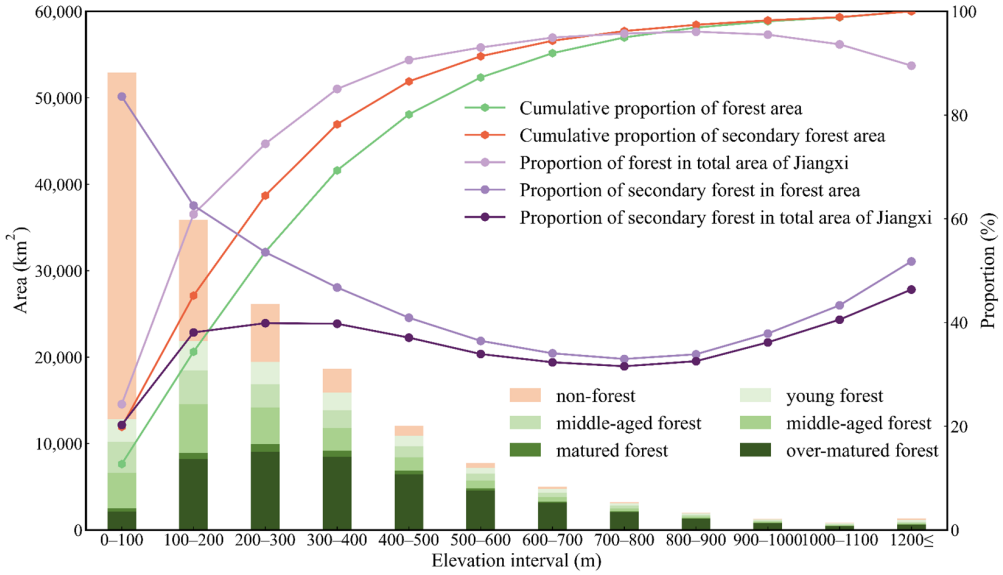


**Figure 10.** Topographical characteristics of secondary forest spatial pattern.

## 4. Discussion

### *4.1. Differences between the Change Detection Algorithms*

As expected, the fundamental logic of the algorithms examined in the present study had a significant impact on the SFA maps. The magnitude threshold-based MACD and VCT showed lower commission and higher omission rates due to the inaccurate thresholds of the different forests [45,68,69]. This study decreased the impact by using the 95% confidence interval calculated from accurate secondary forest samples. LT and VCT were influenced by the logic of using a timing compositing image for observations across year; e.g., the peak of the growing season [41]. The statistical boundary-based CCDC was mainly influenced by false changes due to its sensitivity to land use changes [33]. On the other hand, the different algorithms detected different categories of disturbance. For example, subtle changes in land cover were only detected by CCDC, as the other algorithms were more adept at detecting abrupt changes. In addition, MACD, VCT, and LT only use one band or index as opposed to the multiple bands or indices used in CCDC. The spectral indices chosen were important due to the multispectral expression of some disturbances [34,36,70].

The present study further analyzed differences between the algorithms and other SFA maps by comparing the SFA map produced by CCDC + VCT + LT in 2021 for Jiangxi province to the results obtained by LT, CCDC, and VCT, as well as the map produced by the GPYP dataset. Overall, the results shown in the SFA map from the ensemble model CCDC + VCT + LT were far more comprehensive than those shown in the other maps. In particular, the outputs of the LT, CCDC, and VCT algorithms were missing some key elements. The results of the LT and CCDC algorithms, in contrast to those of the VCT,

were discrete rather than clustered. CCDC + VCT + LT provided more information on the distribution of SFA (Figure 11) compared to the individual algorithms. In addition, records for artificial afforestation in the Statistical Yearbook indicated that GPYP underestimated the area of secondary forest in Jiangxi province. GPYP estimated a total plantation area in 1987–2019 of 3.36 $\times$ $10^4$ $km^2$, whereas the actual artificial afforestation area was 10.09 $\times$ $10^4$ $km^2$. The GPYP map was produced by the LT algorithm. As mentioned above, LT was able to obtain a higher omission rate for forest change detection. In comparison with the GPYP map, the SFA map produced in the present study showed more details, with a smoother boundary for the secondary forest. In particular, GPYP showed little data on the distribution of SFA, particularly in dense forest areas. A comparison of the results of the present study with more products would be difficult without a good regional and worldwide map of SFA.

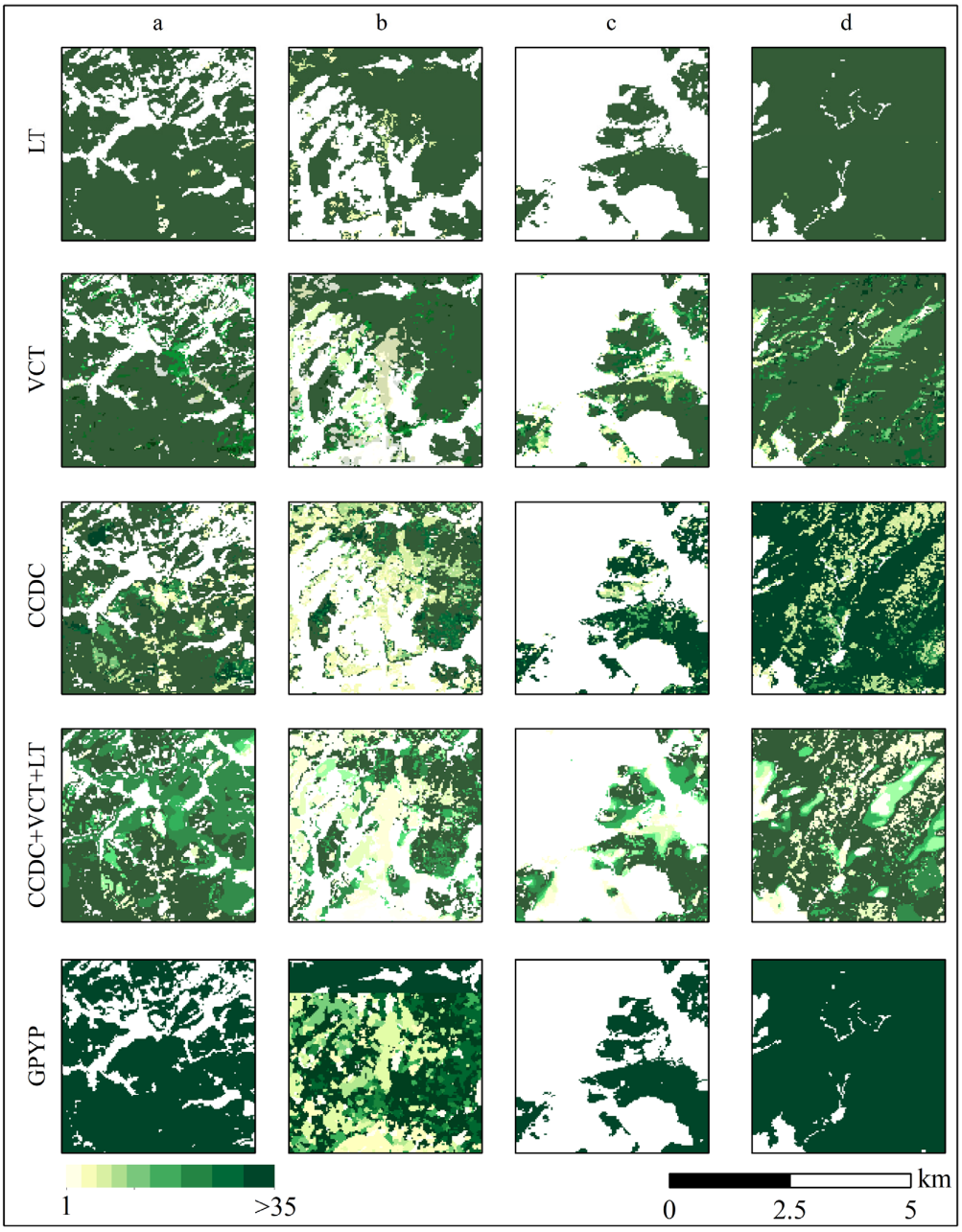


**Figure 11.** The comparison of the SFA maps produced by CCDC + VCT + LT; only LT, VCT, and CCDC; and GPYP in the four areas. From left to right in each column, (**a**–**d**) presents the four types of younger, middle-aged, premature forests, and mature forests in Figure 7.

### *4.2. Advantages and Limitations of the Proposed Method*

A combination of algorithms can improve the accuracy of forest dynamics mapping [41]. The proposed ensemble of CCDC + VCT + LT compensated for the high omission rate of LT, lower accuracy of VCT, and high commission rate of CCDC. The different algorithms showed advantages in detecting particular categories of change. The complementary roles of the different algorithms in the ensemble were facilitated by their different fundamental logics. The proposed method can promote algorithm development and take advantage of the various algorithms to accurately predict changes in secondary forests. However, future studies on the large-scale estimation of SFA will need to resolve the issues of algorithm training, multiple algorithms, and calibration. At the same time, various structural parameters of forests, environmental parameters, remote sensing data, tree species, and degrees of disturbance will need to be considered when assessing SFA [71,72].

### *4.3. Implications of the SFA Map Produced in the Present Study*

The SFA map produced in the present study can act as a significant reference for future studies on forestry and ecosystem services. While afforestation has been implemented in Jiangxi province over the last three decades, the locations and distribution of forests remain unclear. The present study produced a map of secondary forest and forest regrowth (afforestation), thereby revealing the recent spatial and temporal characteristics of secondary forests. The present study can facilitate the improvement of forestry, forest management, and forestry policy. The results of the present study provide input data with higher spatiotemporal resolution for machine learning to estimate forest structures, such as forest height, biomass, canopy density, and stock volume [20,73,74]. In addition, the carbon stocks of secondary forests, particularly subtropical forests, increase with increasing forest age [75]. The SFA data provide a foundation for the estimation of the carbon cycle of secondary forests. The accurate estimation of carbon stocks is a critical step for achieving regional carbon neutrality in Jiangxi province.

## 5. Conclusions

The present study first assessed four time-series change detection algorithms and five developed ensemble models for detecting forest regrowth with dense Landsat time-series data. The optimal proposed ensemble model with CCDC + VCT + LT showed the best performance, with a commission rate of 13.85% and an omission rate of 23.53%. The 2021 SFA map of Jiangxi province was validated from reference forest samples and statistical data with an accuracy represented by $R^2$ = 0.87 and RMSE = 3.17 years. The estimated secondary forest area from 1987 to 2020 in Jiangxi province accounted for 53.47% of the total forest cover, and the average and median ages of the secondary forest were 18 and 17 years, respectively. The comparison between this final SFA map and other SFA maps showed that the optimal ensemble model could compensate for the drawbacks of individual algorithms with the stacked approach. Improved SFA maps can be obtained through the incorporation of additional observation data from forest types and various satellites.

**Author Contributions:** The concept of this study was initially developed by S.Z. and S.Q.; J.Y. and S.H. provided the inventory data from their institute; K.L. and H.X. provided the necessary processing of the data; J.L. and M.H. gave some useful suggestions for writing the paper. All authors have read and agreed to the published version of the manuscript.

**Funding:** The Water Conservancy Science and Technology Project of Jiangxi Province, China (no. 202124ZDKT25), and the National Natural Science Foundation of China (nos 41867012 and 42201438).

**Data Availability Statement:** The data from this study could be provided to readers interested in the relevant research period. Please contact the corresponding author S.Q. with a reasonable request.

**Conflicts of Interest:** The authors declare that they have no conflict of interest.

## Appendix A

**Table A1.** The list of datasets used in this study.

| Data Name | Objective | Period | Spatial Resolution | Sources/Providers |
|---|---|---|---|---|
| Landsat Collection 1 Level-1 | Detecting forest regrowth | 1986–2021 | 30 m | United States Geological Survey (USGS)/GEE [49] |
| World Cover 2020 | Generating the basic forest map | 2020 | 10 m | [55] |
| ESRI 2020 Land Cover | | 2020 | 10 m | [56] |
| GlobeLand 30 | | 2020 | 30 m | [54] |
| First group of forest samples | Assessment of algorithms and ensembles | 2020 | — | Jiangxi Provincial Department of Forestry |
| Second group of forest samples | Validation of the SFA map | 2020/2006 | — | Jiangxi Provincial Department of Forestry |
| Statistical data for the artificial afforestation area | Comparison with the SFA map | 1986–2020 | — | Jiangxi Provincial Bureau of Statistics/Jiangxi Provincial Department of Forestry |
| Global map of planting years of plantations (GPYP) | | 1987–2019 | 30 m | [58] |
| NASA Shuttle Radar Topography Mission (SRTM) | Spatial pattern | 2010 | 30 m | [57] |

**Table A2.** Omission and commission rate errors for individual algorithms and ensemble models.

| Scheme | Omission Rate (%) | Commission Rate (%) | Scheme | Omission Rate (%) | Commission Rate (%) |
|---|---|---|---|---|---|
| CCDC | 37.65 | 15.69 | CCDC + VCT + LT | 23.53 | 13.85 |
| VCT | 49.41 | 16.28 | CCDC + VCT + MACD | 3.53 | 31.71 |
| LT | 93.75 | 16.67 | VCT + CCDC | 23.71 | 17.19 |
| MACD | 7.29 | 38.20 | VCT + CCDC + MACD | 5.88 | 48.75 |
| CCDC + VCT | 24.71 | 14.06 | | | |

## References


1. Xie, X.Y.; Li, A.N.; Jin, H.A. The Simulation Models of the Forest Carbon Cycle on a Large Scale: A Review. *Shengtai Xuebao/Acta Ecol. Sin.* **2018**, *38*, 41–54. [CrossRef]
2. Canadell, J.G.; Le Quéré, C.; Raupach, M.R.; Field, C.B.; Buitenhuis, E.T.; Ciais, P.; Conway, T.J.; Gillett, N.P.; Houghton, R.A.; Marland, G. Contributions to Accelerating Atmospheric $CO_2$ Growth from Economic Activity, Carbon Intensity, and Efficiency of Natural Sinks. *Proc. Natl. Acad. Sci. USA* **2007**, *104*, 18866–18870. [CrossRef] [PubMed]
3. Zhao, X.; Ma, X.; Chen, B.; Shang, Y.; Song, M. Challenges toward Carbon Neutrality in China: Strategies and Countermeasures. *Resour. Conserv. Recycl.* **2022**, *176*, 105959. [CrossRef]
4. Rocha, R.; Ovaskainen, O.; López-Baucells, A.; Farneda, F.Z.; Sampaio, E.M.; Bobrowiec, P.E.D.; Cabeza, M.; Palmeirim, J.M.; Meyer, C.F.J. Secondary Forest Regeneration Benefits Old-Growth Specialist Bats in a Fragmented Tropical Landscape. *Sci. Rep.* **2018**, *8*, 3819. [CrossRef]
5. Chen, Z.; Huang, M.; Xiao, C.; Qi, S.; Du, W.; Zhu, D.; Altan, O. Integrating Remote Sensing and Spatiotemporal Analysis to Characterize Artificial Vegetation Restoration Suitability in Desert Areas: A Case Study of Mu Us Sandy Land. *Remote Sens.* **2022**, *14*, 4736. [CrossRef]
6. Poorter, L.; Bongers, F.; Aide, T.M.; Almeyda Zambrano, A.M.; Balvanera, P.; Becknell, J.M.; Boukili, V.; Brancalion, P.H.S.; Broadbent, E.N.; Chazdon, R.L.; et al. Biomass Resilience of Neotropical Secondary Forests. *Nature* **2016**, *530*, 211–214. [CrossRef] [PubMed]
7. Fehse, J.; Hofstede, R.; Aguirre, N.; Paladines, C.; Kooijman, A.; Sevink, J. High Altitude Tropical Secondary Forests: A Competitive Carbon Sink? *For. Ecol. Manag.* **2002**, *163*, 9–25. [CrossRef]
8. Chave, J.; Andalo, C.; Brown, S.; Cairns, M.A.; Chambers, J.Q.; Eamus, D.; Fölster, H.; Fromard, F.; Higuchi, N.; Kira, T.; et al. Tree Allometry and Improved Estimation of Carbon Stocks and Balance in Tropical Forests. *Oecologia* **2005**, *145*, 87–99. [CrossRef]
9. Chen, J.; Chen, W.; Liu, J.; Cihlar, J.; Gray, S. Annual Carbon Balance of Canada's Forests during 1895–1996. *Glob. Biogeochem. Cycles* **2000**, *14*, 839–849. [CrossRef]
10. He, L.; Chen, J.M.; Zhang, S.; Gomez, G.; Pan, Y.; McCullough, K.; Birdsey, R.; Masek, J.G. Normalized Algorithm for Mapping and Dating Forest Disturbances and Regrowth for the United States. *Int. J. Appl. Earth Obs. Geoinf.* **2011**, *13*, 236–245. [CrossRef]

11. Ju, W.M.; Chen, J.M.; Harvey, D.; Wang, S. Future Carbon Balance of China's Forests under Climate Change and Increasing $CO_2$. *J. Environ. Manag.* **2007**, *85*, 538–562. [CrossRef] [PubMed]
12. Turner, D.P.; Ritts, W.D.; Law, B.E.; Cohen, W.B.; Yang, Z.; Hudiburg, T.; Campbell, J.L.; Duane, M. Scaling Net Ecosystem Production and Net Biome Production over a Heterogeneous Region in the Western United States. *Biogeosciences* **2007**, *4*, 597–612. [CrossRef]
13. Wang, S.; Zhou, L.; Chen, J.; Ju, W.; Feng, X.; Wu, W. Relationships between Net Primary Productivity and Stand Age for Several Forest Types and Their Influence on China's Carbon Balance. *J. Environ. Manag.* **2011**, *92*, 1651–1662. [CrossRef] [PubMed]
14. Wang, S.; Chen, J.M.; Ju, W.M.; Feng, X.; Chen, M.; Chen, P.; Yu, G. Carbon Sinks and Sources in China's Forests during 1901–2001. *J. Environ. Manag.* **2007**, *85*, 524–537. [CrossRef]
15. Zhang, F.; Chen, J.M.; Pan, Y.; Birdsey, R.A.; Shen, S.; Ju, W.; He, L. Attributing Carbon Changes in Conterminous U.S. Forests to Disturbance and Non-Disturbance Factors from 1901 to 2010. *J. Geophys. Res. Biogeosci.* **2015**, *117*, 109–119. [CrossRef]
16. Chambers, J.Q.; Asner, G.P.; Morton, D.C.; Anderson, L.O.; Palace, M.; Saatchi, S.S.; Espı, F.D.B. Regional Ecosystem Structure and Function: Ecological Insights from Remote Sensing of Tropical Forests. *Trends Ecol. Evol.* **2007**, *22*, 411–423. [CrossRef] [PubMed]
17. Dai, M.; Zhou, T.; Ynag, L.; Jia, G. Spatial pattern of forest ages in China retrieved from national-level inventory and remotes ensing imageries. *Geogr. Res.* **2011**, *30*, 172–184. [CrossRef]
18. Kimes, D.S.; Nelson, R.F.; Salas, W.A.; Skole, D.L. Mapping Secondary Tropical Forest and Forest Age from SPOT HRV Data. *Int. J. Remote Sens.* **1999**, *20*, 3625–3640. [CrossRef]
19. Yu, Z.; Zhao, H.; Liu, S.; Zhou, G.; Fang, J.; Yu, G.; Tang, X.; Wang, W.; Yan, J.; Wang, G.; et al. Mapping Forest Type and Age in China's Plantations. *Sci. Total Environ.* **2020**, *744*, 140790. [CrossRef]
20. Zhang, C.; Ju, W.; Chen, J.M.; Li, D.; Wang, X.; Fan, W.; Li, M.; Zan, M. Mapping Forest Stand Age in China Using Remotely Sensed Forest Height and Observation Data. *J. Geophys. Res. Biogeosci.* **2014**, *119*, 1163–1179. [CrossRef]
21. Zhang, Y.; Yao, Y.; Wang, X.; Liu, Y.; Piao, S. Mapping Spatial Distribution of Forest Age in China. *Earth Space Sci.* **2017**, *4*, 108–116. [CrossRef]
22. Chen, B.; Xiao, X.; Wu, Z.; Yun, T.; Kou, W.; Ye, H.; Lin, Q.; Doughty, R.; Dong, J.; Ma, J.; et al. Identifying Establishment Year and Pre-Conversion Land Cover of Rubber Plantations on Hainan Island, China Using Landsat Data during 1987–2015. *Remote Sens.* **2018**, *10*, 1240. [CrossRef]
23. Prates-Clark, C.d.C.; Lucas, R.M.; dos Santos, J.R. Implications of Land-Use History for Forest Regeneration in the Brazilian Amazon. *Can. J. Remote Sens.* **2009**, *35*, 534–553. [CrossRef]
24. Silva Junior, C.H.L.; Heinrich, V.H.A.; Freire, A.T.G.; Broggio, I.S.; Rosan, T.M.; Doblas, J.; Anderson, L.O.; Rousseau, G.X.; Shimabukuro, Y.E.; Silva, C.A.; et al. Benchmark Maps of 33 Years of Secondary Forest Age for Brazil. *Sci. Data* **2020**, *7*, 269. [CrossRef]
25. Carreiras, J.M.B.; Jones, J.; Lucas, R.M.; Shimabukuro, Y.E. Mapping Major Land Cover Types and Retrieving the Age of Secondary Forests in the Brazilian Amazon by Combining Single-Date Optical and Radar Remote Sensing Data. *Remote Sens. Environ.* **2017**, *194*, 16–32. [CrossRef]
26. Dibs, H.; Idrees, M.O.; Alsalhin, G.B.A. Hierarchical Classification Approach for Mapping Rubber Tree Growth Using Per-Pixel and Object-Oriented Classifiers with SPOT-5 Imagery. *Egypt. J. Remote Sens. Space Sci.* **2017**, *20*, 21–30. [CrossRef]
27. Reyes-Palomeque, G.; Dupuy, J.M.; Portillo-Quintero, C.A.; Andrade, J.L.; Tun-Dzul, F.J.; Hernández-Stefanoni, J.L. Mapping Forest Age and Characterizing Vegetation Structure and Species Composition in Tropical Dry Forests. *Ecol. Indic.* **2021**, *120*, 106955. [CrossRef]
28. Xie, S.; Wang, W.; Liu, Q.; Meng, J.; Zhao, T.; Huang, G. Estimation of Forest Stand Parameters Using SPOT-5 Satellite Images and Topographic Information. *Forestry* **2017**, 2017100017. [CrossRef]
29. Zhang, Q.; Pavlic, G.; Chen, W.; Latifovic, R.; Fraser, R.; Cihlar, J. Deriving Stand Age Distribution in Boreal Forests Using SPOT VEGETATION and NOAA AVHRR Imagery. *Remote Sens. Environ.* **2004**, *91*, 405–418. [CrossRef]
30. Chazdon, R.L.; Broadbent, E.N.; Rozendaal, D.M.A.; Bongers, F.; Zambrano, A.M.A.; Aide, T.M.; Balvanera, P.; Becknell, J.M.; Boukili, V.; Brancalion, P.H.S.; et al. Carbon Sequestration Potential of Second-Growth Forest Regeneration in the Latin American Tropics. *Sci. Adv.* **2016**, *2*, e1501639. [CrossRef]
31. Chen, G.; Thill, J.-C.; Anantsuksomsri, S.; Tontisirin, N.; Tao, R. Stand Age Estimation of Rubber (*Hevea brasiliensis*) Plantations Using an Integrated Pixel- and Object-Based Tree Growth Model and Annual Landsat Time Series. *ISPRS J. Photogramm. Remote Sens.* **2018**, *144*, 94–104. [CrossRef]
32. Razak, J.A.b.A.; Shariff, A.R.b.M.; Ahmad, N.b.; Ibrahim Sameen, M. Mapping Rubber Trees Based on Phenological Analysis of Landsat Time Series Data-Sets. *Geocarto Int.* **2018**, *33*, 627–650. [CrossRef]
33. Awty-Carroll, K.; Bunting, P.; Hardy, A.; Bell, G. An Evaluation and Comparison of Four Dense Time Series Change Detection Methods Using Simulated Data. *Remote Sens.* **2019**, *11*, 2779. [CrossRef]
34. Huang, C.; Goward, S.N.; Masek, J.G.; Thomas, N.; Zhu, Z.; Vogelmann, J.E. An Automated Approach for Reconstructing Recent Forest Disturbance History Using Dense Landsat Time Series Stacks. *Remote Sens. Environ.* **2010**, *114*, 183–198. [CrossRef]
35. Thomas, N.E.; Huang, C.; Goward, S.N.; Powell, S.; Rishmawi, K.; Schleeweis, K.; Hinds, A. Validation of North American Forest Disturbance Dynamics Derived from Landsat Time Series Stacks. *Remote Sens. Environ.* **2011**, *115*, 19–32. [CrossRef]
36. Kennedy, R.E.; Yang, Z.; Cohen, W.B. Detecting Trends in Forest Disturbance and Recovery Using Yearly Landsat Time Series: 1. LandTrendr—Temporal Segmentation Algorithms. *Remote Sens. Environ.* **2010**, *114*, 2897–2910. [CrossRef]

37. Kennedy, R.E.; Yang, Z.; Cohen, W.B.; Pfaff, E.; Braaten, J.; Nelson, P. Spatial and Temporal Patterns of Forest Disturbance and Regrowth within the Area of the Northwest Forest Plan. *Remote Sens. Environ.* **2012**, *122*, 117–133. [CrossRef]
38. Zhu, Z.; Woodcock, C.E. Continuous Change Detection and Classification of Land Cover Using All Available Landsat Data. *Remote Sens. Environ.* **2014**, *144*, 152–171. [CrossRef]
39. Zhao, Z.; Meng, Y.; Yue, A.; Huang, Q.; Kong, Y.; Yuan, Y.; Liu, X.; Lin, L.; Zhang, M. Review of Remotely Sensed Time Series Data for Change Detection. *Yaogan Xuebao/J. Remote Sens.* **2016**, *20*, 1110–1125. [CrossRef]
40. Zhu, Z. Change Detection Using Landsat Time Series: A Review of Frequencies, Preprocessing, Algorithms, and Applications. *ISPRS J. Photogramm. Remote Sens.* **2017**, *130*, 370–384. [CrossRef]
41. Cohen, W.B.; Healey, S.P.; Yang, Z.; Stehman, S.V.; Brewer, C.K.; Brooks, E.B.; Gorelick, N.; Huang, C.; Hughes, M.J.; Kennedy, R.E.; et al. How Similar Are Forest Disturbance Maps Derived from Different Landsat Time Series Algorithms? *Forests* **2017**, *8*, 98. [CrossRef]
42. Healey, S.P.; Cohen, W.B.; Yang, Z.; Kenneth Brewer, C.; Brooks, E.B.; Gorelick, N.; Hernandez, A.J.; Huang, C.; Joseph Hughes, M.; Kennedy, R.E.; et al. Mapping Forest Change Using Stacked Generalization: An Ensemble Approach. *Remote Sens. Environ.* **2018**, *204*, 717–728. [CrossRef]
43. Hislop, S.; Jones, S.; Soto-Berelov, M.; Skidmore, A.; Haywood, A.; Nguyen, T.H. A Fusion Approach to Forest Disturbance Mapping Using Time Series Ensemble Techniques. *Remote Sens. Environ.* **2019**, *221*, 188–197. [CrossRef]
44. Chen, B.; Jin, Y.; Brown, P. Automatic Mapping of Planting Year for Tree Crops with Landsat Satellite Time Series Stacks. *ISPRS J. Photogramm. Remote Sens.* **2019**, *151*, 176–188. [CrossRef]
45. Danylo, O.; Pirker, J.; Lemoine, G.; Ceccherini, G.; See, L.; McCallum, I.; Hadi; Kraxner, F.; Achard, F.; Fritz, S. A Map of the Extent and Year of Detection of Oil Palm Plantations in Indonesia, Malaysia and Thailand. *Sci. Data* **2021**, *8*, 96. [CrossRef]
46. Liu, C.; Huang, H.; Zhang, Q.; Chen, X.; Xu, X.; Xu, H.; Cheng, X. Arctic's Man-Made Impervious Surfaces Expanded by over Two-Thirds in the 21st Century. *Sci. Bull.* **2022**, *67*, 1425–1429. [CrossRef]
47. Xu, H.; Qi, S.; Li, X.; Gao, C.; Wei, Y.; Liu, C. Monitoring Three-Decade Dynamics of Citrus Planting in Southeastern China Using Dense Landsat Records. *Int. J. Appl. Earth Obs. Geoinf.* **2021**, *103*, 102518. [CrossRef]
48. National Forestry and Grassland Administration. *Chinese Forest Resources Report*; China Forestry Publishing House: Beijing, China, 2019; ISBN 978-7-5038-9982-9.
49. Gorelick, N.; Hancher, M.; Dixon, M.; Ilyushchenko, S.; Thau, D.; Moore, R. Google Earth Engine: Planetary-Scale Geospatial Analysis for Everyone. *Remote Sens. Environ.* **2017**, *202*, 18–27. [CrossRef]
50. Zhu, Z.; Wang, S.; Woodcock, C.E. Remote Sensing of Environment Improvement and Expansion of the Fmask Algorithm: Cloud, Cloud Shadow, and Snow Detection for Landsats 4–7, 8, and Sentinel 2 Images. *Remote Sens. Environ.* **2015**, *159*, 269–277. [CrossRef]
51. Lei, X.D.; Tang, M.P.; Lu, Y.C.; Hong, L.X.; Tian, D.L. Forest Inventory in China: Status and Challenges. *Int. For. Rev.* **2009**, *11*, 52–63. [CrossRef]
52. Xie, X.; Wang, Q.; Dai, L.; Su, D.; Wang, X.; Qi, G.; Ye, Y. Application of China's National Forest Continuous Inventory Database. *Environ. Manag.* **2011**, *48*, 1095–1106. [CrossRef] [PubMed]
53. Li, Y.; Li, C.; Li, M.; Liu, Z. Influence of Variable Selection and Forest Type on Forest Aboveground Biomass Estimation Using Machine Learning Algorithms. *Forests* **2019**, *10*, 1073. [CrossRef]
54. Jun, C.; Ban, Y.; Li, S. China: Open Access to Earth Land-Cover Map. *Nature* **2014**, *514*, 434. [CrossRef]
55. Zanaga, D.; Van De Kerchove, R.; De Keersmaecker, W.; Souverijns, N.; Brockmann, C.; Quast, R.; Wevers, J.; Grosu, A.; Paccini, A.; Vergnaud, S.; et al. ESA WorldCover 10 m 2020 V100. 2021. Available online: https://doi.org/10.5281/zenodo.5571936 (accessed on 1 May 2022).
56. Karra, K.; Kontgis, C.; Statman-Weil, Z.; Mazzariello, J.C.; Mathis, M.; Brumby, S.P. Global Land Use / Land Cover with Sentinel 2 and Deep Learning. In Proceedings of the IEEE International Geoscience and Remote Sensing Symposium IGARSS, Brussels, Belgium, 12–16 July 2021; pp. 4704–4707. [CrossRef]
57. Farr, T.G.; Rosen, P.A.; Caro, E.; Crippen, R.; Duren, R.; Hensley, S.; Kobrick, M.; Paller, M.; Rodriguez, E.; Roth, L.; et al. The Shuttle Radar Topography Mission. *Rev. Geophys.* **2007**, *45*, RG2004. [CrossRef]
58. Du, Z.; Yu, L.; Yang, J.; Xu, Y.; Chen, B.; Peng, S.; Zhang, T.; Fu, H.; Harris, N.; Gong, P. A Global Map of Planting Years of Plantations. *Sci. Data* **2022**, *9*, 141. [CrossRef]
59. Diao, J.; Feng, T.; Li, M.; Zhu, Z.; Liu, J.; Biging, G.; Zheng, G.; Shen, W.; Wang, H.; Wang, J.; et al. Use of Vegetation Change Tracker, Spatial Analysis, and Random Forest Regression to Assess the Evolution of Plantation Stand Age in Southeast China. *Ann. For. Sci.* **2020**, *77*, 27. [CrossRef]
60. López García, M.J.; Caselles, V. Mapping Burns and Natural Reforestation Using Thematic Mapper Data. *Geocarto Int.* **1991**, *6*, 31–37. [CrossRef]
61. Arévalo, P.; Bullock, E.L.; Woodcock, C.E.; Olofsson, P. A Suite of Tools for Continuous Land Change Monitoring in Google Earth Engine. *Front. Clim.* **2020**, *2*, 576–740. [CrossRef]
62. White, J.C.; Wulder, M.A.; Hobart, G.W.; Luther, J.E.; Hermosilla, T.; Griffiths, P.; Coops, N.C.; Hall, R.J.; Hostert, P.; Dyk, A.; et al. Pixel-Based Image Compositing for Large-Area Dense Time Series Applications and Science. *Can. J. Remote Sens.* **2014**, *40*, 192–212. [CrossRef]
63. Shen, W.; Li, M.; Wei, A. Spatio-Temporal Variations in Plantation Forests' Disturbance and Recovery of Northern Guangdong Province Using Yearly Landsat Time Series Observations (1986–2015). *Chin. Geogr. Sci.* **2017**, *27*, 600–613. [CrossRef]

64. Cohen, W.B.; Yang, Z.; Healey, S.P.; Kennedy, R.E.; Gorelick, N. A LandTrendr Multispectral Ensemble for Forest Disturbance Detection. *Remote Sens. Environ.* **2018**, *205*, 131–140. [CrossRef]
65. Hu, S.Y.; Pang, Y.; Meng, S.L.; Yue, C.R. Annual Forest Disturbance Detection Using Time Series Landsat 8 OLI Data. *For. Res.* **2020**, *33*, 65–72. [CrossRef]
66. Zhou, D.; Liu, S.; Oeding, J.; Zhao, S. Forest Cutting and Impacts on Carbon in the Eastern United States. *Sci. Rep.* **2013**, *3*, 3547. [CrossRef] [PubMed]
67. Hua, J.; Chen, G.; Yu, L.; Ye, Q.; Jiao, H.; Luo, X. Improved Mapping of Long-Term Forest Disturbance and Recovery Dynamics in the Subtropical China Using All Available Landsat Time-Series Imagery on Google Earth Engine Platform. *IEEE J. Sel. Top. Appl. Earth Obs. Remote Sens.* **2021**, *14*, 2754–2768. [CrossRef]
68. Zhang, Y.; Shen, W.; Li, M.; Lv, Y. Integrating Landsat Time Series Observations and Corona Images to Characterize Forest Change Patterns in a Mining Region of Nanjing, Eastern China from 1967 to 2019. *Remote Sens.* **2020**, *12*, 3191. [CrossRef]
69. Fang, L.; Yang, J.; Zhang, W.; Zhang, W.; Yan, Q. Combining Allometry and Landsat-Derived Disturbance History to Estimate Tree Biomass in Subtropical Planted Forests. *Remote Sens. Environ.* **2019**, *235*, 111423. [CrossRef]
70. Zhu, Z.; Woodcock, C.E.; Holden, C.; Yang, Z. Generating Synthetic Landsat Images Based on All Available Landsat Data: Predicting Landsat Surface Reflectance at Any given Time. *Remote Sens. Environ.* **2015**, *162*, 67–83. [CrossRef]
71. Du, Y.; Li, M.; Fan, W.; Wang, B. Estimation of Forest Stand Age Based on GWR Model and Forest Fire Remote Sensing Data. *Sci. Silvae Sin.* **2019**, *55*, 184–194. [CrossRef]
72. Cutler, D.R.; Edwards, T.C.; Beard, K.H.; Cutler, A.; Hess, K.T.; Gibson, J.; Lawler, J.J. Random forests for classification in ecology. *Ecology* **2007**, *88*, 2783–2792. [CrossRef]
73. Huang, W.; Min, W.; Ding, J.; Liu, Y.; Hu, Y.; Ni, W.; Shen, H. Forest Height Mapping Using Inventory and Multi-Source Satellite Data over Hunan Province in Southern China. *For. Ecosyst.* **2022**, *9*, 100006. [CrossRef]
74. Peng, D.; Zhang, H.; Liu, L.; Huang, W.; Huete, A.R.; Zhang, X.; Wang, F.; Yu, L.; Xie, Q.; Wang, C.; et al. Estimating the Aboveground Biomass for Planted Forests Based on Stand Age and Environmental Variables. *Remote Sens.* **2019**, *11*, 2270. [CrossRef]
75. Pugh, T.A.M.; Lindeskog, M.; Smith, B.; Poulter, B.; Arneth, A.; Haverd, V.; Calle, L. Role of Forest Regrowth in Global Carbon Sink Dynamics. *Proc. Natl. Acad. Sci. USA* **2019**, *116*, 4382–4387. [CrossRef] [PubMed]